Driving Rain, Rain Absorption, and Rainwater Runoff for Evaluating Water Leakage Risks in Building Envelopes

Jan Carmeliet, Ph.D. **Bert Blocken, Ph.D.**

ABSTRACT

Driving rain is one of the major sources of moisture in building envelopes causing moisture damages. Depending on the capillary absorptivity, moisture storage of surface materials, and the rate of driving rain, a water film forms and runs down the wall, leading to an important accumulation of water and an increased risk for rain penetration and leakage. In this paper the driving rain distribution in time and space and the occurrence of runoff for different building typologies is analyzed: a tall and a long low-rise building, a building with an opening, and a tall building with an underpass. A computational fluid dynamics (CFD)-based model for driving rain is combined with a heat and moisture transport model for capillary active materials and a runoff model is added based on the thin film theory. Driving rain and runoff intensities are highest at corners and edges of the building, while a sheltered zone at the bottom of the building may exist. Runoff depends also on the moisture transport characteristics of the surface material. The use of semi-empirical relations based on driving rain coefficients for evaluating the driving rain intensity is critically analyzed. It is concluded that the driving rain coefficient should be handled with care, since it is found not to be a constant during time for a given place on the building facade.

INTRODUCTION

Wind-driven rain (or driving rain), i.e., rain that is carried by the wind and given a horizontal velocity component, is one of the most important moisture sources for building envelopes and must be adequately taken into account when designing the building facade. If the outer surface is made of capillary active materials, the material first absorbs the rainwater during a certain period, until capillary saturation is attained at the surface. Then water accumulates at the outer surface, forming a thin sticking film, which thickness grows in time and will finally run down the facade due to gravity. The film running down may penetrate into cracks and joints, leading to preferential water ingress and, consequently, a higher risk for deterioration due to frost, corrosion rot, and chemical and biological degradation processes.

A proper design of building envelopes regarding driving rain clearly requires an appropriate methodology consisting of four steps: (1) the evaluation of the driving rain distribution in time and space over the facade, (2) the determination of the amount of rainwater runoff, (3) the analysis of the risk of water penetration through joints and cracks, and (4) the evaluation of the moisture damage risk and formulation of mitigating measures. A first attempt to evaluate the moisture damage risk by rain infiltration following these different steps is presented by Teasdale-St-Hilaire et al. (2003). Based on driving rain data obtained by computational fluid dynamics (CFD) on a low-rise building, rainwater leakage was first quantified in a rain penetration chamber, followed by a study in a climatic chamber of the wetting and drying characteristics of walls that were subject to small leakage failures.

This paper focuses on the first two steps of the methodology. (1) An extension of driving rain knowledge is proposed that allows one to determine the distribution in space and time of driving rain on different building typologies using the practical numerical simulation method for driving rain, as developed by Blocken and Carmeliet (2000a, 2000b, 2002). The use

Jan Carmeliet is a full professor at the Laboratory of Building Physics, Department of Civil Engineering, Katholieke Universiteit Leuven, Belgium, and at the Building Physics Group, Faculty of Building and Architecture, Eindhoven University of Technology, The Netherlands. **Bert Blocken** is a post-doctoral researcher at the Laboratory of Building Physics, Department of Civil Engineering, Katholieke Universiteit Leuven, Belgium.

of semi-empirical relations for driving rain evaluation are critically analyzed and discussed. (2) The risk of rain penetration, such as at interface details (e.g., windows), clearly depends on the accumulation of rainwater running down the facade. The evaluation of rainwater runoff requires the coupling of a driving rain model, a model for heat and moisture transport taking into account possible buffering by capillary water uptake by envelope materials, and a model for runoff. In this paper, an integrated model based on driving rain, heat and moisture transport, and runoff simulation is presented.

DRIVING RAIN ESTIMATION

Until recently, information on driving rain on buildings was gathered by employing either an experimental or a semi-empirical approach. Based on experimental observations, it was shown that both the free-driving rain (i.e., without buildings present) and the driving rain on buildings increase approximately proportionally with wind speed and horizontal rainfall intensity. In order to account for the effect of wind direction, the factor $\cos\theta$ is usually added to the product of wind speed and horizontal rainfall intensity, where θ is the angle between the wind direction and the line normal to the wall (multiplying with $\cos\theta$ corresponds to using the component of the wind speed normal to the wall). To take into account local phenomena induced by the topography and by the building itself, a driving rain coefficient α is introduced, which leads to the relation,

$$R_{dr} = \alpha \cdot U \cdot R_h \cdot \cos\theta \,, \qquad (1)$$

where U is the wind speed, R_{dr} is the driving rain intensity, and R_h is the horizontal rain intensity (i.e., through a horizontal plane). This relation indicates that the product $U{\cdot}R_h{\cdot}\cos\theta$, also referred to as driving rain index, can be seen as a measure for possible driving rain. For free driving rain (no influence of buildings or topography), the driving rain coefficient equals approximately 0.222 s/m. The weakness of this semi-empirical method is the determination of the driving rain coefficient α on buildings, as the entire complexity of the interaction between driving rain and the building is to be integrated in this single value. Measurements by Lacy (1965), Ishizaki et al. (1970), Schwarz (1973), Sandin (1991), Henriques (1992), Flori (1992), Künzel (1993), Hens and Ali Mohamed (1994), Straube and Burnett (1997), and others indicate that driving rain coefficients vary considerably with the size of the building and show a large variation across the building facade: values from 0.02 s/m (9% of the free coefficient 0.222 s/m) to 0.26 s/m (120% of 0.222 s/m) have been found. In most heat-air-moisture (HAM) simulation models, the driving rain coefficient is an input parameter that does not vary with the climatic data. In one-dimensional simulation models, a constant value for the driving rain coefficient is commonly assumed.

As research efforts continued to reveal the inherent complexity of the driving rain problem, researchers realized that further achievements were to be found through numerical analyses. In the past decade, CFD has been introduced in the area. A number of researchers have employed CFD to study the trajectories of raindrops in the calculated wind flow pattern around a building and to determine the driving rain amount falling onto the building facade (Choi 1993; Wisse 1994; Sankaran and Paterson 1995; Lakehal et al. 1995; Karagiozis et al. 1997; van Mook et al. 1997; van Mook 1999; Etyemezian et al. 2000). Based on their investigations, a practical numerical simulation method for driving rain has been developed (Blocken and Carmeliet 2000a, 2000b). The method allows the calculation of both the spatial and temporal distribution of driving rain on buildings based on generally available climatic data (wind speed, wind direction, rainfall intensity). It has been validated and it has been found to yield fairly accurate results for the case of a low-rise building and for different rain events (Blocken and Carmeliet 2000a, 2002).

The quantities that are used to describe the driving rain load in the numerical approach are the specific catch ratio η_d (for one raindrop diameter d) and the catch ratio η (for all raindrop diameters).

$$\eta_d(t) = \frac{R_{dr}(d,t)}{R_h(d,t)} \qquad \eta(t) = \frac{R_{dr}(t)}{R_h(t)} \qquad (2)$$

where

$R_{dr}(d,t)$ and $R_h(d,t)$ = the specific driving rain intensity and specific horizontal rainfall intensity (i.e., through a horizontal plane) for raindrops with diameter d (L/m²h or mm/h)

$R_{dr}(t)$ and $R_h(t)$ = the same quantities but integrated over all raindrop diameters taking into account the raindrop spectrum

The catch ratio is a complicated function of space and time. The six basic influencing parameters for the catch ratio are: (1) building geometry (including environment topology), (2) position on the building envelope, (3) (reference) wind speed, (4) wind direction, (5) (horizontal) rainfall intensity, and (6) (horizontal) raindrop size distribution. Reference wind speed U_{10} (m/s) and wind direction φ_{10} (degrees from north) refer to values at 10 m height in the upstream undisturbed flow. Horizontal rainfall intensity R_h and horizontal raindrop size distribution $f_h(d)$ refer to values through a horizontal plane in the undisturbed flow field.

In this analysis, four simple typologies of stand-alone buildings are analyzed (Figure 1). The first type is a tall building of 30 m height. The second type is a long, low-rise building. In type 3, an opening is situated in the middle of a low-rise building. Type 4 is the building of type 1 with an underpass. Types 3 and 4 are studied in order to analyze the influence of the gap on local driving rain exposure.

DRIVING RAIN AND RUNOFF MODELING

To calculate the driving rain load and runoff on a building facade for a given climate data set, the following six steps have to be executed.

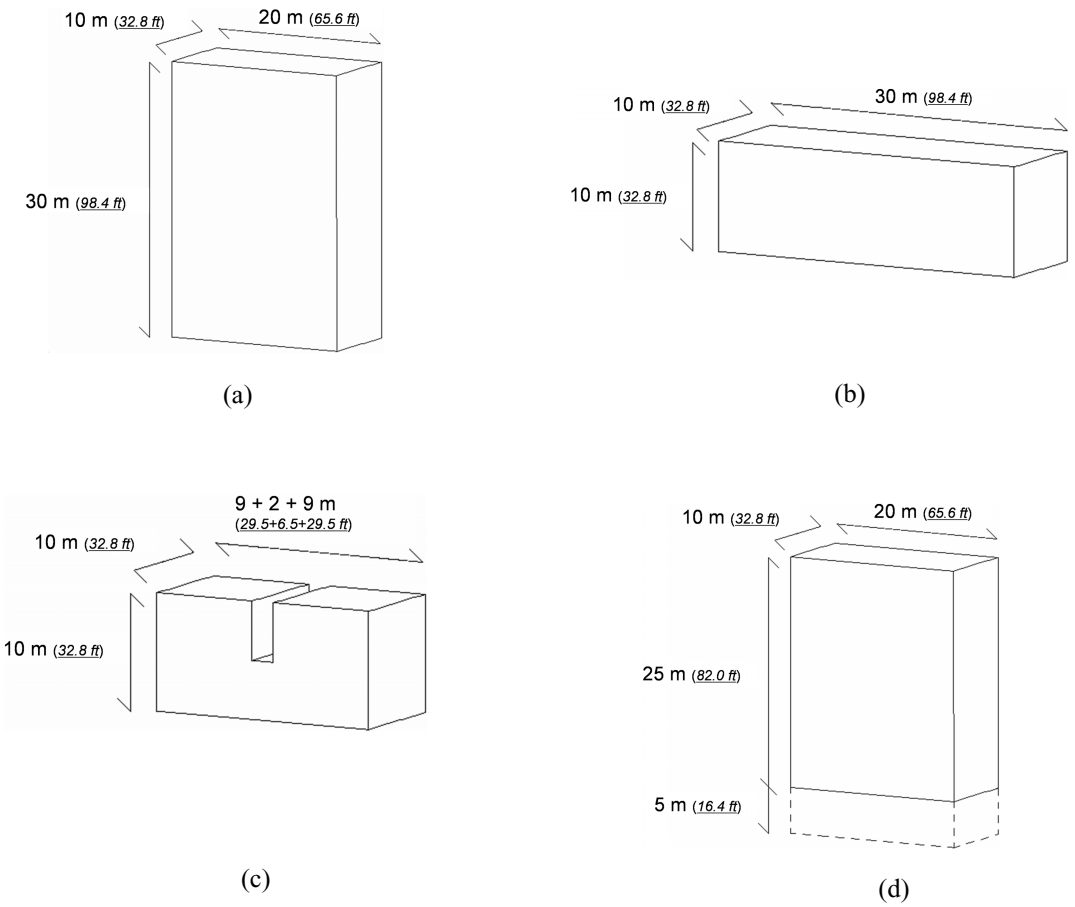

Figure 1 *Building typologies analyzed in this paper: (a) tall building, (b) long low-rise building, (c) building with opening, and (d) tall building with underpass.*

Steady-State Wind Flow Pattern

The steady-state wind flow pattern around the building is calculated using CFD. The Reynolds averaged Navier-Stokes (RANS) equations and the continuity equation are solved using the commercial code Fluent 5.4. Closure is obtained by employing a version of the k-ε turbulence model. The undisturbed vertical wind flow profile is assumed to follow a logarithmic function with the surface roughness and reference wind speed U_{10} as parameters.

Raindrop Trajectories

With the given wind flow pattern, the raindrop trajectories can be calculated. The raindrops are injected from a high level above the ground. The drops are dragged by the wind, receive a horizontal velocity component, and may finally hit the building. The trajectory of the raindrop is calculated using three-dimensional Lagrangian particle tracking. Droplets with a diameter of 0.5 to 6 mm are injected in the wind flow field with wind speeds ranging from 0 to 10 m/s. In general, it is observed that for smaller drops and at higher wind speed, the trajectories are more inclined and their distortion near the building becomes more pronounced. For larger drops (higher inertia) and at a lower wind speed, the trajectories are less inclined and more rectilinear (Blocken and Carmeliet 2002).

Catch Ratio

First the specific catch ratio η_d (for one raindrop diameter) will be calculated. By integration of the specific catch ratio over the raindrop spectrum, the catch ratio will be obtained. To calculate the specific catch ratio, raindrops with a given radius are released in a dense horizontal rectangular grid in the upstream wind. A large number of the numerically released drops hits the building facade. Based on the configuration of the raindrop trajectories, the specific catch ratio η_d is obtained (Choi 1993; Blocken and Carmeliet 2000a, 2002).

The catch ratio η for a position on the facade is obtained by multiplying η_d for each raindrop diameter d with the fraction of these drops in the spell and integrating over all raindrop diameters.

$$\eta = \int_d f_h(d)\eta_d(d)dd \tag{3}$$

where

$f_h(d)$ = the raindrop size distribution through a horizontal plane.

For the present study, the empirical raindrop size distribution of Best (1950) is adopted. This size distribution shows a one-to-one relationship between the horizontal rainfall intensity and the raindrop spectrum. This means that, recalling the six basic parameters of the catch ratio mentioned above, and with a fixed wind direction and a fixed position on the building facade, the two variables wind speed and horizontal rainfall intensity unambiguously define the catch ratio.

The distribution of the catch ratio over the facade for the different building typologies is given in Figure 2. The horizontal rain intensity is 5 mm/h (0.20 in./h) in a wind field with a reference speed of 5 m/s (16.4 ft/s). The figures indicate that driving rain intensities are much higher at the upper edges and corners for all building types. The catch ratio at the upper edge and corners only slightly increases with the height of the building. For the tall building a zone exists at the bottom of the building that is completely sheltered from driving rain. The sheltered zone disappears for the lower buildings types (Figures 2b and 2c). Driving rain intensities increase locally at the opening in the building (Figure 2c), especially at the lower

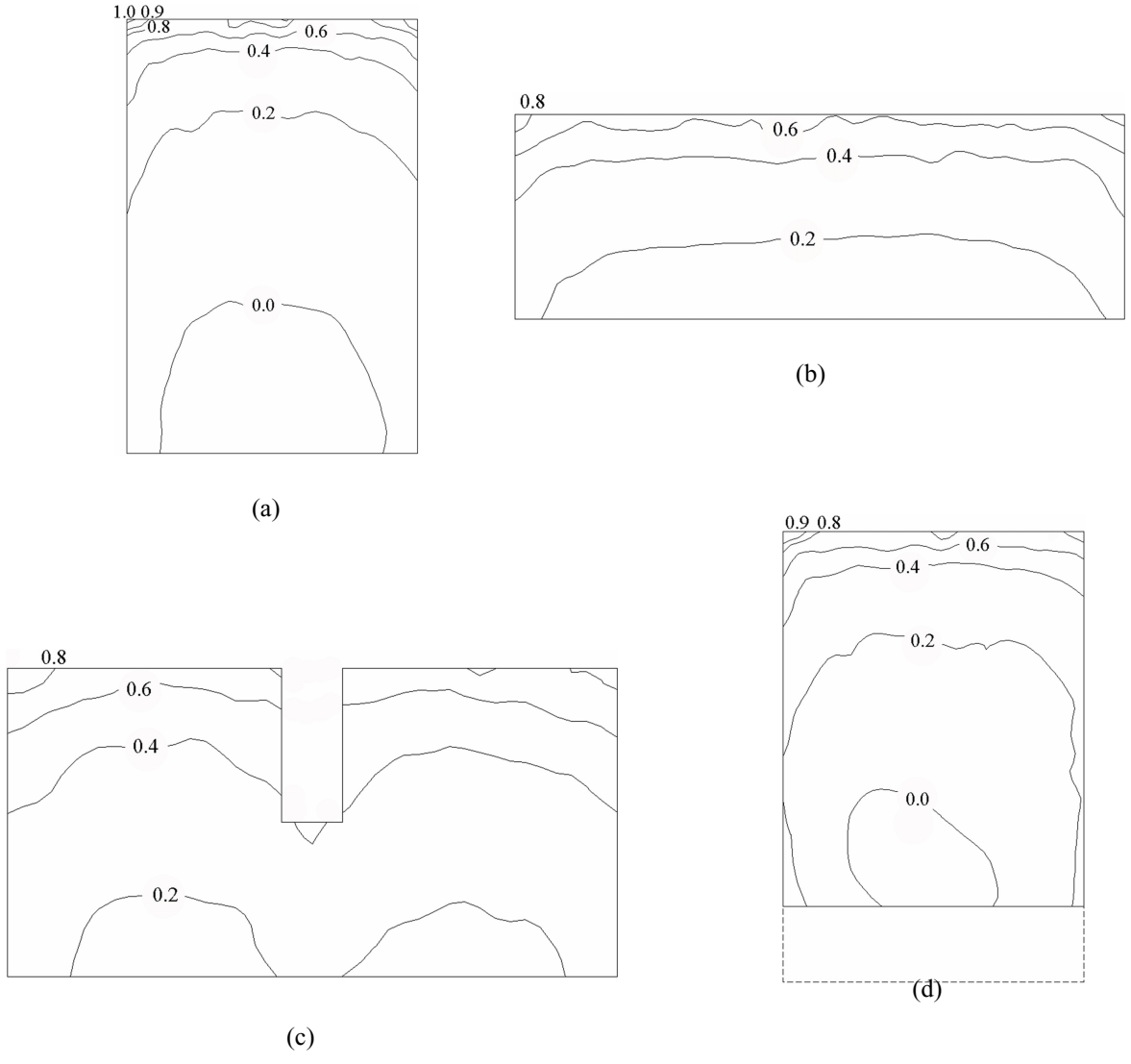

Figure 2 *Numerical calculation results: contours of the catch ratio over the facade (*R_h *= 5 mm/h,* U_{10} *= 5 m/s) (*R_h *= 0.197 in./h,* U_{10} *= 16.4 ft/s).*

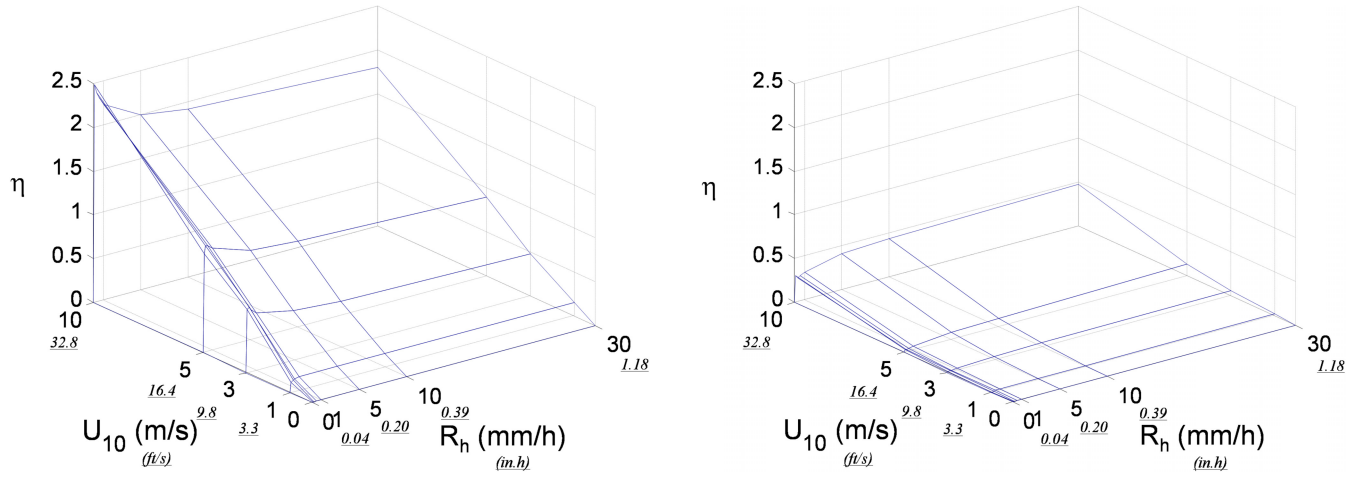

Figure 3 *Numerically calculated catch ratio as a function of wind speed and horizontal rainfall intensity for two positions of building type "a." The wind direction is perpendicular to the facade.*

edge. The higher catch ratio can be explained by the local increase in wind speed at this point. The presence of the underpass (Figure 2d) leads to a small shift of the sheltered zone upward. Note that although locally high wind speeds are present in the underpass, this does not lead to driving rain in the middle of the building. The underpass, however, causes the sheltered zone to shrink laterally due to higher catch ratios at the edges of the building.

Zooming into two selected positions at the facade (position 1 at the upper corner edge of building "a" and position 2 in the middle of this building), the dependency of the catch ratio on wind speed and horizontal rainfall intensity is given in Figures 3a and 3b. At the corner (position 1), the catch ratio increases almost linearly, with the wind speed reaching values of more than two. The highest catch ratios are observed for low horizontal rainfall intensities, which is an indication of the sweeping effect (both upward and sideward) that is typical for small rain droplets at building corners (Blocken and Carmeliet 2002). The catch ratio in the middle of the building is much lower and the highest values are attained during rain spells with high horizontal rainfall intensity and high wind speed (which rarely occurs in reality).

Driving Rain Events

Once the catch ratio as a function of wind speed and horizontal rainfall intensity is known, the driving rain intensities for transient rain events, with fluctuating wind speed and horizontal rainfall intensity, can be determined. Therefore, the considered time period (i.e., one year) is divided into a number of equidistant time steps, each of which is considered steady-state. With each of these time steps (index i), the corresponding measured data of reference wind speed U_i (= U_{10}) and horizontal rainfall intensity R_{hi} that are available from a weather station are associated. Note that even minor variations in topography and landscape can have an important influence on the microclimatic wind speed and horizontal rainfall intensity close to the building. Transformation of weather station data to meso- and microscale values, to be used in the driving rain simulation, is still subject of (future) research. Here, a simplified approach is adopted, where the inlet wind profile is consistent with the surface roughness.

For each time step i, the corresponding catch ratio can be calculated by employing the steady-state technique (that is: steps 1-3 in the model) for the couple (U_i, R_i). To reduce the computational expense, the catch ratio will not be calculated for every time step but only for a selected set of couples (U_i, R_i). Intermediate values are obtained by linear interpolation in the U-R-η charts (see Figure 3), giving the dependency of the catch ratio on wind speed and horizontal rainfall intensity. To study driving rain for different topographic places, "characteristic" climates have to be used, which are derived from an extensive set of climatic data measured over several years. Precipitation amounts are, however, rarely included in such data, since most characteristic data are commonly used for simulations of energy consumption and not for moisture transfer. In this paper, the design reference years (DRY) for Essen, Germany, are used (Grunewald 1997). It is recognized that these data have some limitations, since the used selection method for the rain data does not necessarily reproduce the average duration of precipitation (Künzel 1993). Equation 1 shows that the driving rain index $U \cdot R_h \cdot \cos\theta$ is a measure for possible driving rain. The proportionality factor, called driving rain coefficient α, is usually assumed to be independent of climatic data (wind speed, horizontal rainfall intensity, raindrop size distribution). Measurements indicate that driving rain coefficients may vary considerably with the size of the building and show a large variation across the building facade: values from 0.02 s/m to 0.26 s/m have been found. No information is

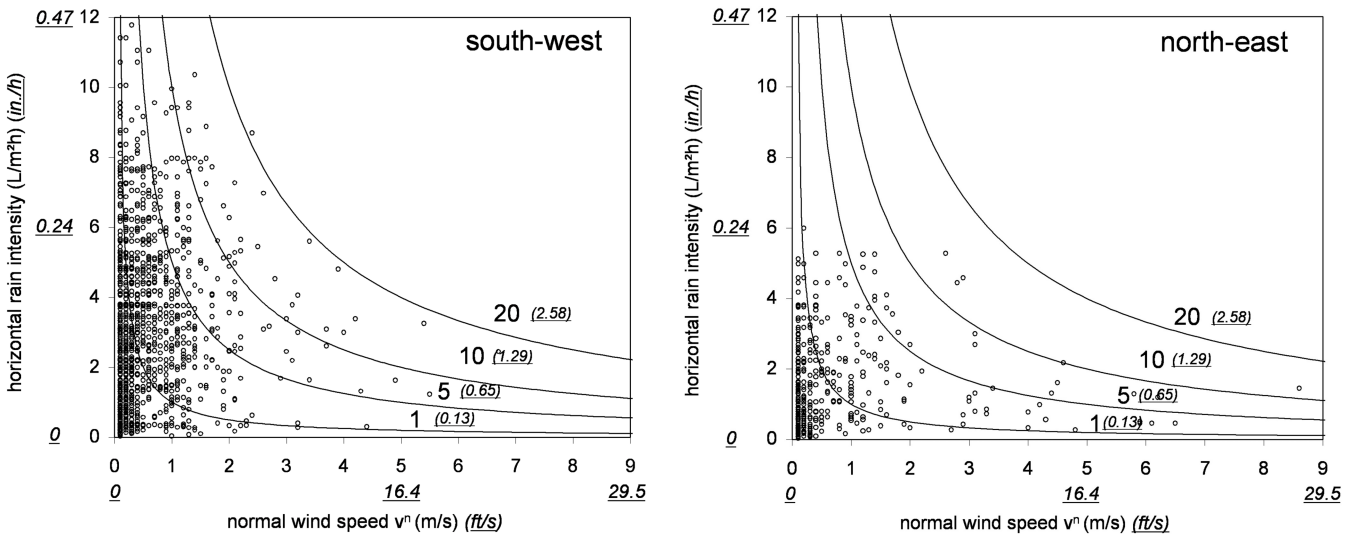

Figure 4 *The hourly horizontal rain intensity as a function of the wind speed normal to the building for the southwest and northeast orientations.*

given about possible temporal variation of the driving rain coefficient. In most heat-air-moisture simulation models, the driving rain coefficient is an input parameter assumed to be constant in time, only to depend on the place on the facade. These assumptions will now be analyzed in more detail.

Figures 4a and 4b give the hourly horizontal rain intensity as function of the hourly wind speed normal to the building for two facade orientations: southwest and northeast. These orientations are known to generally show the highest driving rain intensities in western Europe. The lines in the graph are isolines for the driving rain index. The graphs show that the wind speed is mostly low during rain, leading to moderate values of the driving rain index. High driving rain indices are the result of a combination of high horizontal rainfall intensity and low wind speed or vice versa. High values of the rain index for the northeast orientation are due to higher wind speeds.

Figures 5a to 5d give the driving rain intensities as a function of the driving rain index $U \cdot R_h \cdot \cos\theta$. The lines define isolines for the driving rain coefficient α. First, it is noted that the driving rain coefficient at the top corner (building "a," southwest orientation, Figure 5a) is clearly not a constant, but ranges from values of 0.11 to 0.25. Using a linear curve fit, an average a value of 0.218 is obtained. It is remarkable that the upper limit of the driving rain coefficient almost equals the value of 0.222, which means that the top corner catches as much driving rain as in the free field (with no building present). Values lower than 0.2 indicate that due to the particular wind flow pattern around the building, a lower deposition of driving rain is attained compared to the free field. Lower values of the driving rain coefficient α can be attributed to low values of the horizontal rainfall intensity. Figure 5b gives the driving rain intensities as a function of the driving rain index $U \cdot R_h \cdot \cos\theta$ for the middle of building 'a'. The driving rain coefficient here ranges from 0 to 0.034, with an average α value of 0.018. The lower α values are due to the blocking effect of the building. The blocking effect refers to the fact that the building, due to its presence, slows down the wind speed upstream of it. Figure 5c gives the driving rain intensity as a function of the driving rain index $U \cdot R_h \cdot \cos\theta$ for the northeast orientation (corner of building "a"). Compared to the southwest orientation, a lower number of driving rain events are observed. The driving rain coefficient ranges, as for the southeast orientation, from 0.11 to 0.25, with a lower average α value of 0.203. Figure 5d gives the driving rain intensity as a function of the driving rain index $U \cdot R_h \cdot \cos\theta$ at a location just beneath the gap in building "c" (see Figure 1). The facade is oriented to the southeast. The driving rain coefficient ranges from 0.04 to 0.1, with an average α value of 0.09. This particular behavior may be explained by the high wind speeds close to the gap in the building.

These results show that the driving rain coefficient α may range from 0 to 0.25 for a tall building. The driving rain coefficient is not a constant for a given place on the facade, since it depends in a complex way on wind speed, horizontal rainfall intensity, and raindrop size distribution. All of these observations question the correctness of Equation 1 when using a constant driving rain coefficient for a given place on the facade. It is concluded that the driving rain coefficient, although frequently used in HAM-simulations, should be handled with care, since the parameter is found to be not a constant during time for a given place on a building facade.

Heat and Moisture Transport

The physical model solving the heat and moisture transport in a capillary active wall that has been used is the one developed at the Laboratory of Building Physics based on the

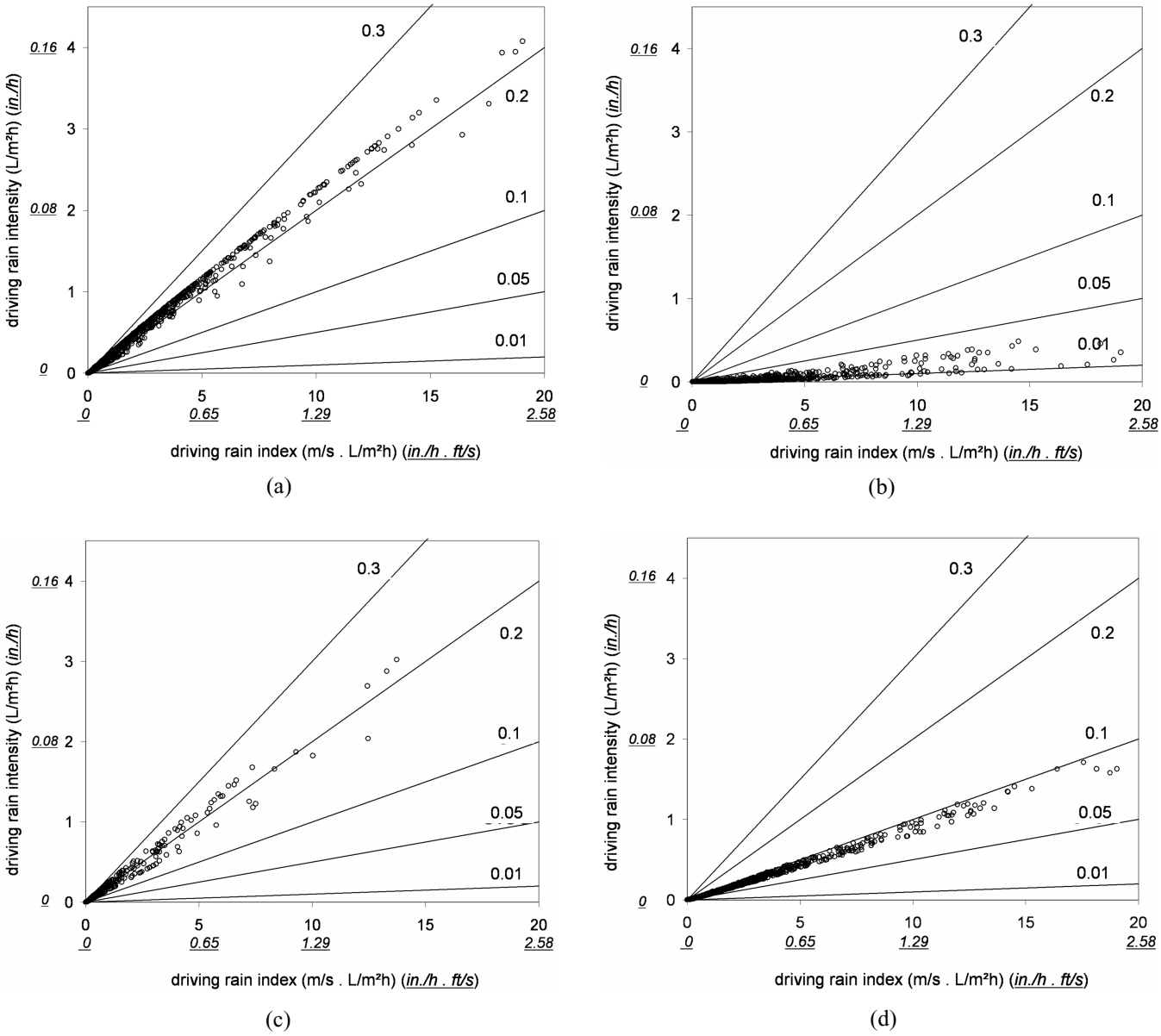

Figure 5 *The driving rain intensities as a function of the driving rain index $U{\cdot}R_h{\cdot}\cos\theta$: (a) top corner of building "a," orientation southwest; (b) middle of building "a," orientation southwest; (c) top corner of building "a," orientation northeast; (d) beneath the gap of building "c," orientation southwest.*

simulation code by Janssen (2002). First, the one-dimensional simulation is presented for the heat and moisture response of a cavity brick wall at the corner of the building of type "a." The insulation layer and inside wall are simplified to a constant internal boundary coefficient $h_i = 0.7$ W/m²K. Further, focusing on driving rain, possible vapor transport to the inside is neglected. The moisture retention curve and permeability are determined from standard experiments using the material determination methodology as proposed by Carmeliet and Roels (2001, 2002). Two types of brick are considered. For simplicity, the moisture transport properties are described by the capillary absorption coefficient and capillary moisture content. The capillary moisture content is here defined as the moisture content when the moisture front reaches the height of a specimen in a free capillary absorption experiment. The capillary absorption coefficient is a measure for the speed of water uptake (slope of the uptake curve versus square root of time). The first type of brick (A) is characterized by a high water absorption coefficient $A_{cap} = 0.59$ kg/m^2.s$^{0.5}$ and high capillary moisture content $w_{cap} = 225$ kg/m^3, which means that the brick will quickly take up driving rain and can buffer a high quantity of driving rain. The second type of brick shows a

moderate capillary absorption coefficient A_{cap} = 0.14 kg/m^2·s$^{0.5}$ and a low capillary moisture content w_{cap} = 82 kg/m^3, which means that the brick can only buffer a small quantity of driving rain.

Figures 6a to 6d give time sequences of the average moisture content, the moisture content at the surface, and the driving rain index (corner position of building "a," southwest orientation). When the moisture content at the surface equals the capillary moisture content, runoff occurs. Figures 6a and 6b show the results during winter for brick A with high moisture buffering capacity and brick B with low moisture buffering capacity. Note that when runoff occurs, the surface moisture content equals the average moisture content for both bricks, which means that the brick is over its total depth capillary saturated. The high levels of average moisture content are due to a combined effect of water uptake during rain and of supercooling condensation during nighttime. Brick B shows higher variations in average moisture content due to its lower moisture buffering capacity. During summer, brick A buffers all driving rain during the time sequence shown (Figure 6c). Brick B, with a lower moisture buffering capacity, shows one instance of runoff during the same time sequence (Figure 6d). The low average moisture content during no-rain periods is due to an extensive drying of the brick during sunny and warm days.

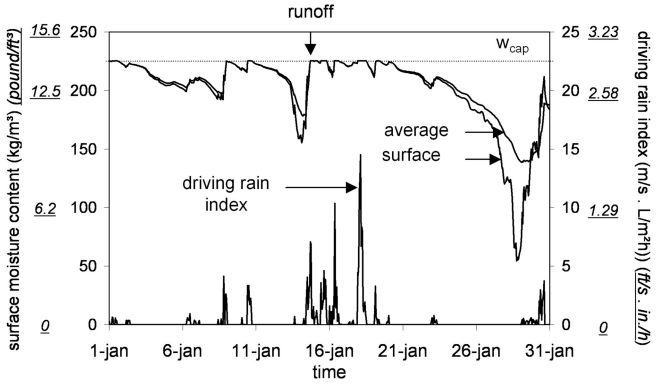

(a)

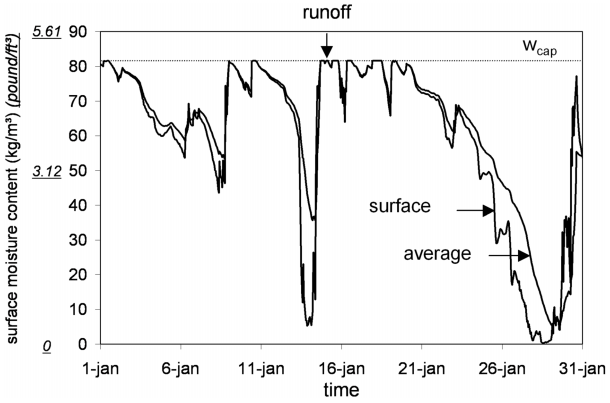

(b)

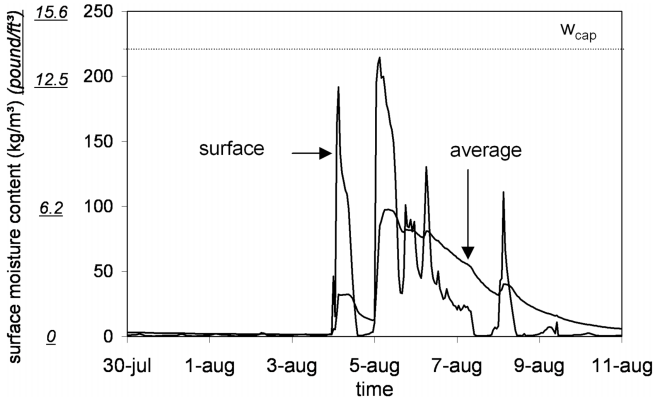

(c)

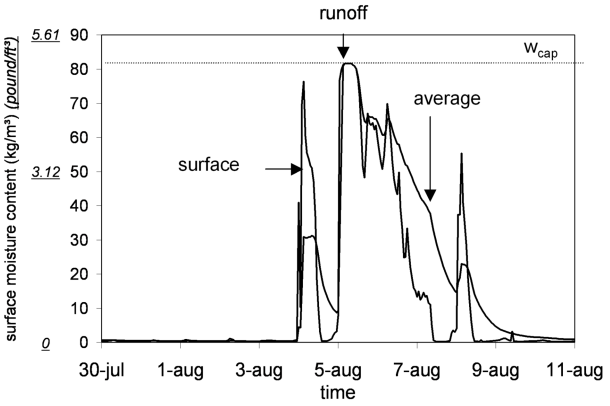

(d)

Figure 6 *Time sequence of the average moisture content, the moisture content at the surface, and the driving rain index: (a) southwest, top corner of building "a," material A, winter; (b) southwest, top corner of building "a," material B, winter; (c) southwest, top corner of building "a," material A, summer; (d) southwest, top corner of building "a," material B, summer.*

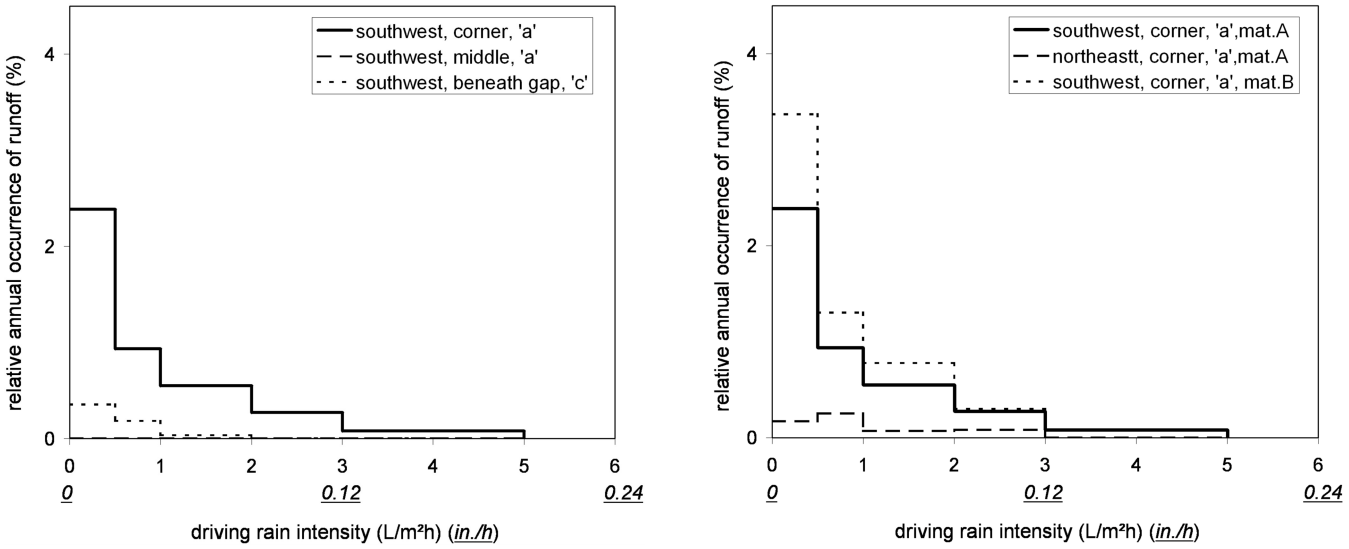

Figure 7 *Annual frequency distributions of runoff intensity for different places on the facade, different orientations, and different materials A and B.*

Figures 7a and 7b give the annual frequency distributions of runoff intensity for different places on the facade, different orientations, and different materials. Runoff most frequently shows low intensities (lower than 3 L/m^2·h) (0.073 gal/ft²). Material B shows higher runoff intensities compared to material A. The distributions are most extreme for the top corner. Lower runoff intensities are found beneath the gap. The middle of the building is highly sheltered from high driving rain intensities, and no runoff occurs. The northeast orientation receives less driving rain and, consequently, a lower occurrence of runoff is observed.

Table 1 gives the annual percentage of time (*T*) that runoff occurs, and the total amount of runoff (*Q*) over one year for material A for the different locations on the building types and for different orientations. Table 2 provides the same information for material B. The following observations are made:

- The influence of the type of building is rather limited. Although the top corners of the two tall buildings show the highest frequencies and the largest amount of runoff, these values are only slightly larger than those at the top corners of the two low-rise buildings.
- The influence of the position on the building on the frequency and amount of runoff is very much pronounced. These values are clearly more pronounced at those positions that experience the highest driving rain exposure. At the middle of the building facade, practically no runoff is observed. It is important to note that none of these buildings has a roof overhang and that the presence of such a feature will shift the position of maximum runoff frequency and amount to a lower position at the facade.
- The influence of the building orientation: southwest- and northwest-oriented facades clearly show the largest percentages and amount of runoff.
- The influence of the building material: runoff is considerably more pronounced for material B (lower absorption coefficient and lower capillary moisture content) than for material A.

Runoff Model

The rainfall runoff model is developed as an extension of the Nusselt solution for fluid flow (Ruyer-Quil and Manneville 1998). The following assumptions are adopted:

1. The film flow is uniform (fingering phenomena do not occur)
2. The film is thin enough for the Reynolds number to be negligible
3. The Reynolds number is small enough to avoid ripples
4. The film thickness is large enough so that surface forces are negligible.
5. The fluid in the film (water) is incompressible and Newtonian
6. The surrounding fluid (air) has zero density and viscosity
7. Surface tension and surface viscosity are neglected
8. Pressure is constant over the film thickness

Figure 8 schematically presents the flow of a fluid film down a vertical plane due to driving rain. The model is derived based on the following two equations:

1. The continuity equation, adapted with the driving rain source term
2. The momentum equation in the z-direction

Table 1. Annual Percentage of Time (*T*) That Runoff Occurs and the Total Amount of Runoff (*Q*) Over One Year for Material A, for the Different Locations on the Building Types and for Different Orientations

	T **%**	***Q*** **L/m²** **gal/ft²**		***T*** **%**	***Q*** **L/m²** ***gal/ft²***		***T*** **%**	***Q*** **L/m²** ***gal/ft²***
 southwest	4.2	245 *6.0*	 southwest	0	0 *0*	 northeast	0.01	0.34 0
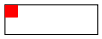 southwest	3.4	201 *4.9*	 southwest	0	0 *0*	 southeast	0.6	44 *1.1*
 southwest	3.2	188 *4.6*	 southwest	0.6	24 *0.6*	 southwest	4.2	245 *6.0*
 southwest	3.6	211 *5.2*	 southwest	0	0 *0*	 northwest	1.9	164 *4.0*

Table 2. Annual Percentage of Time (*T*) That Runoff Occurs and the Total Amount of Runoff (*Q*) Over One Year for Material B, for the Different Locations on the Building Types and for Different Orientations

	T **%**	***Q*** **L/m²** **gal/ft²**		***T*** **%**	***Q*** **L/m²** ***gal/ft²***		***T*** **%**	***Q*** **L/m²** ***gal/ft²***
 southwest	5.8	312 *7.7*	 southwest	0	0 *0*	 northeast	0.7	29 *0.7*
 southwest	4.7	256 *6.3*	 southwest	0.5	0.2 *0*	 southeast	0.8	60 *1.5*
 southwest	4.5	240 *5.9*	 southwest	1.3	42 *1.0*	 southwest	5.8	312 *7.7*
 southwest	4.9	270 *6.6*	 southwest	0	0 *0*	 northwest	2.3	190 *4.7*

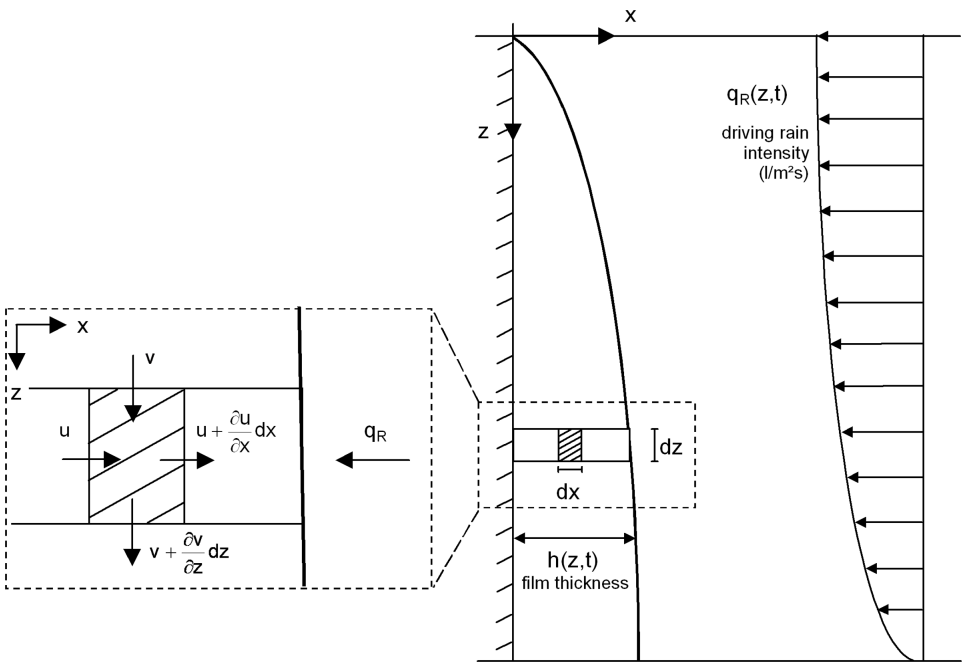

Figure 8 *Schematic presentation and symbols for continuous film runoff caused by driving rain.*

The resulting equation is

$$\frac{\partial h}{\partial t} + \frac{\rho \cdot g}{3 \cdot \mu} \cdot \frac{\partial h^3}{\partial z} - \frac{q_R}{\rho} + \frac{q_{abs}}{\rho} = 0 \,, \qquad (4)$$

where h is the thickness of the film, ρ is the liquid water density, μ is the dynamic water viscosity, q_R is the driving rain intensity, and q_{abs} is the water flux into the material by capillary absorption. Equation 4 is a nonlinear, first-order, hyperbolic differential equation. It can be solved numerically with an upwind finite difference scheme, employing forward differencing in time and backward differencing in space.

Two examples are selected to illustrate rainwater runoff. For simplicity and for illustrating purposes, we focus on a vertical wall made of a noncapillary active material of 2.7 m (8.86 ft) height. In the first example, a high driving rain intensity of q_R = 10 L/m²h (0.394 in./h) is imposed to the upper part of the wall (1 m [3.28 ft] height, see Figure 9a). No rain reaches the lower part. This represents a case where the lower part of the wall is sheltered from driving rain impact and is only wetted by rainwater runoff from the upper part. Figure 9a illustrates the results at different time steps. The wetting front propagates down the wall until a steady state is reached. In the second example, a linearly varying driving intensity is imposed to the material: q_R varies from 10 L/m²h (0.394 in./h) at the top to 1 L/m²h (0.039 in./h) at the bottom. This represents a realistic situation where a driving rain intensity gradient exists over the height of the wall. Figure 9b shows the results. The propagating front is less steep in this case, as the total height of the wall is wetted with driving rain and a film develops at all positions. In both cases, maximum film thickness is about 0.1 mm (0.0039 in.) and a steady state is reached after about one minute.

CONCLUSIONS

1. The evaluation of rainwater runoff is modeled by coupling of a driving rain model based on computational fluid dynamics and particle tracking, a model for heat and moisture transport taking into account possible buffering by capillary water uptake by envelope materials, and a model for runoff based on the thin film theory.

2. Different stand-alone building typologies are analyzed: a tall and a low-rise building, a building with an opening, and a tall building with an underpass. It was observed that the driving rain intensity is highest at the upper edge and at the top corners of the building. The amount of driving rain slightly increases with height of the building. For the tall building, a zone exists that is completely sheltered from driving rain at the bottom of the building. The sheltered zone disappears for the lower building types. Driving rain intensities may increase locally near an opening in a building, especially at the lower edge of this opening where higher wind speeds are found. The presence of the underpass leads to a small shift of the sheltered zone upward. Higher wind speeds in the underpass do not lead to driving rain in the middle of the underpass edge. The underpass does cause the sheltered zone to shrink laterally due to higher driving rain intensity at the edges of the building.

3. Driving rain for all typologies shows most frequently low driving rain intensities (lower than 0.5 L/m^2·h) (0.02 in./h). The middle of the building is more sheltered, especially for high driving rain intensities. The northeast orientation clearly receives less driving rain.

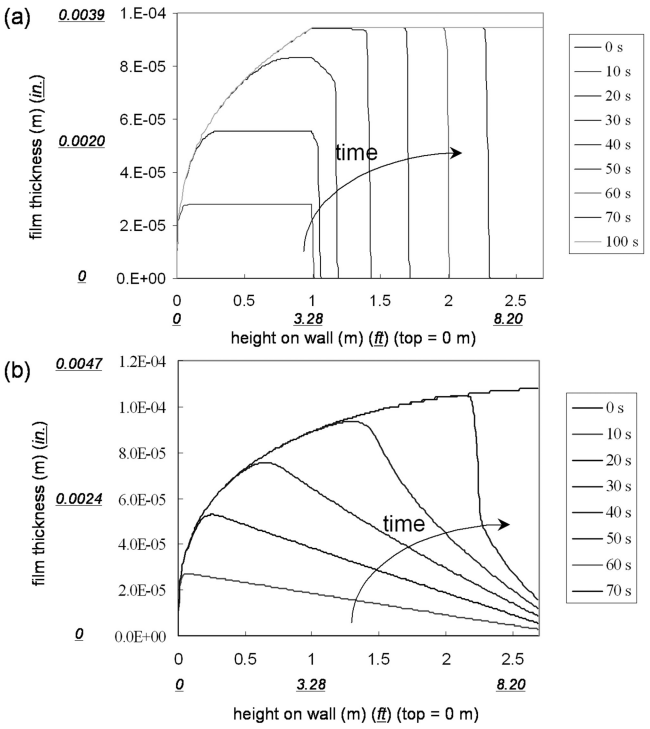

Figure 9 *Film flow down a vertical wall caused by driving rain impact. (a) Driving rain intensity q_R = 10 L/m^{2}h (0.394 in./h) on the upper part (1 m [3.28 ft]) of the wall. (b) Driving rain intensity q_R varies linearly from 10 L/m^{2}h or mm/h (0.394 in./h) at the top to 1 L/m^{2}h or mm/h (0.039 in./h) at the bottom of the wall.*

4. It was shown that the semi-empirical approach, based on the well-known relationship between driving rain, wind speed, and horizontal rainfall (driving rain = driving rain coefficient * wind speed * horizontal rainfall intensity) should be handled with care. The major drawback in using this relationship is the fact that the driving rain coefficient is not a constant, as is usually assumed. It is a complicated function of space and time. The driving rain coefficient is found to range from 0 to 0.25.

5. During winter, a lot of rainwater runoff may occur since the bricks remain at high moisture content caused by important wetting by driving rain and nighttime supercooling condensation and by the limited drying potential. During summer, porous materials with sufficient moisture buffering capacity do not show runoff. The bricks may dry out during sunny and warm days, resulting in a full availability of the moisture buffering capacity during rain. Materials with less moisture buffering capacity may show runoff.

6. Film forming starts when the material reaches the capillary moisture content at the surface. Initially the film does not run down and sticks on the wall. From a certain thickness the film runs down due to gravity. The thickness of the film running down is limited and a steady state is reached after about one minute.

7. The present study has been conducted with hourly data. Preliminary studies by the present authors have indicated that data with a higher temporal resolution are preferred for the study of driving rain and runoff. Unfortunately, the use of hourly data is standard practice in building physics (and in many other research areas) and, therefore, climatic databases typically consist of hourly data. Future studies will benefit from the availability of large databases with at least ten-minute climate data.

8. It is noted that the CFD model for the calculation of the wind flow field has been extensively verified and validated (step 1 in the model) (Blocken 2004). Also, the catch ratio calculation and the calculation of the driving rain amount in space and time (steps 2 to 4) have been validated (Blocken and Carmeliet 2002; Blocken 2004). Future research efforts should focus on the validation of the runoff model. Very little research on this topic has been performed in building physics until now, and the current models for runoff from facades (including the one presented in this paper) are based on a significant number of assumptions. Validating the runoff model constitutes a challenge for the future.

REFERENCES

Best, A.C. 1950. The size distribution of raindrops. *Quarterly Journal of the Royal Meteorological Society* 76:16-36.

Blocken, B., and J. Carmeliet. 2000a. Driving rain on building envelopes—I: Numerical estimation and full-scale experimental verification. *J. Thermal Env. & Bldg. Sci*. 24(1):61-85.

Blocken, B., and J. Carmeliet, J. 2000b. Driving rain on building envelopes—II: Representative experimental data for driving rain estimation. *J. Thermal Env. & Bldg. Sci*. 24(2):89-110.

Blocken, B., and J. Carmeliet. 2002. Spatial and temporal distribution of driving rain on a low-rise building. *Wind Struct.* 5(5):441-462.

Blocken, B. 2004. Wind-driven rain on buildings: Measurements, numerical modelling and applications. Ph.D. thesis, Laboratory of Building Physics, Department of Civil Engineering, Katholieke Universiteit Leuven, 323 p.

Carmeliet J., and S. Roels. 2001. Determination of the isothermal moisture transport properties of porous building materials. *Journal of Thermal Envelope and Building Science* 24:183-210.

Carmeliet J., and S. Roels. 2002. Determination of the moisture capacity of porous building materials. *Journal of Thermal Envelope and Building Science* 25(3):209-237.

Choi, E.C.C. 1993. Simulation of wind-driven-rain around a building. *J. Wind Eng. Ind. Aerod.*, Vol. 46 and 47, pp. 721-729.

Etyemezian, V., C.I. Davidson, M. Zufall, W. Dai, S. Finger, and M. Striegel. 2000. Impingement of rain drops on a tall building. *Atmos. Environ.* 34:2399-2412.

Flori, J.P. 1992. Influence des conditions climatiques sur le mouillage et le séchage d'une façade verticale (in French). Cahiers du CSTB, livraison 332, September 1992, cahier 2606.

Grunewald J. 1997. Diffusiver und konvektiver stoff- und energietransport in kapillarporösen baustoffen. Ph.D. thesis, Technische Universität Dresden, Dresden, Germany.

Henriques, F.M.A. 1992. Quantification of wind-driven rain—An experimental approach. *Building Research and Information* 20(5):295-297.

Hens, H., and F. Ali Mohamed. 1994. Preliminary results on driving rain estimation. Contribution to the IEA annex 24, Task 2—Environmental conditions, T2-B-94/02.

Ishizaki, H., Y. Mitsuta, and Y. Sano. 1970. Rainfall deposit on a wall of a building in a storm. Bulletin of the Disaster Prevention Research Institute, Kyoto University, 20(2), No. 174, (December 1970), pp. 95-103.

Janssen, H. 2002. The influence of soil moisture transfer on building heat loss via the ground, Ph.D. thesis, Faculty of Applied Sciences, Department of Civil Engineering, Katholieke Universiteit Leuven, Belgium.

Karagiozis, A., G. Hadjisophocleous, and S. Cao. 1997. Wind-driven rain distributions on two buildings. *J. Wind Eng. Ind. Aerod.*, Vol. 67 and 68, pp. 559-572.

Künzel, H.M. 1993. Rain loads on building elements. Contribution to the IEA-Annex-24 meeting, Report T2-D-93/02, Holzkirchen, October 1993.

Lacy, R.E. 1965. Driving-rain maps and the onslaught of rain on buildings. RILEM/CIB Symp. on Moisture Problems in Buildings, Rain Penetration, Helsinki, August 16-19, Vol. 3, paper 3-4.

Lakehal, D., P.G. Mestayer, J.B. Edson, S. Anquetin, and J.-F. Sini,. 1995. Eulero-Lagrangian simulation of raindrop trajectories and impacts with the urban canopy. *Atmos. Environ.* 29(23):3501-3517.

Ruyer-Quil, C., and P. Manneville. 1998. Modeling film flows down inclined planes. *The European Physical Journal* B6(2):277-292.

Sandin, K. 1991. Skalmurskonstruktionens fukt- och temperaturbetingelser. Rapport R43: 1991 Byggforskningsradet, Stockholm, Sweden.

Sankaran, R., and D.A. Paterson. 1995. Computation of rain falling on a tall rectangular building. Proc. 9ICWE, New Delhi, India, pp. 2127-2137.

Schwarz, B. 1973. Witterungsbeanspruchung von Hochhausfassaden (in German). HLH (Heizung, Lüftung/Klimatechnik, Haustechnik), Bd. 24, Nr. 12, pp. 376-384.

Straube, J.F., and E.F.P. Burnett. 1997. Driving rain and masonry veneer. ASTM Symp. on Water Leakage Through Building Facades, Orlando, March 17 1996. Special Technical Publication, ASTM STP 1314, Philadelphia, 1997, pp. 73-87.

Teasdale-St-Hilaire A, D. Derome, and P. Fazio. 2003. Development of an experimental methodology for the simulation of wetting due to rain infiltration for building envelope testing. Research in Building Physics. Eds. Carmeliet J, Hens H, Vermeir G. Swets & Zeitlinger, Lisse.

Van Mook, F.J.R. 1999. Measurements and simulations of driving rain on the Main Building of the TUE. Proc. 5th Symp. Build. Phys. Nordic Countries, Gothenburg, Sweden, pp. 377-384.

Van Mook, F.J.R., M.H. De Wit, and J.A. Wisse. 1997. Computer simulation of driving rain on building envelopes. Proc. 2EACWE, Genova, Italy, pp. 1059-1066.

Wisse, J.A. 1994. Driving rain, a numerical study. *Proceedings of 9th Symposium on Building Physics and Building Cli-matology.* Dresden, September.